Materials Advances

ROYAL SOCIETY OF CHEMISTRY

COMMUNICATION

View Article Online
View Journal | View Issue

Cite this: *Mater. Adv.*, 2023, 4, 3708

Received 4th July 2023,
Accepted 29th July 2023

DOI: 10.1039/d3ma00364g

rsc.li/materials-advances

Aerosol-assisted chemical vapour deposition of highly efficient mixed anatase-rutile TiO_2 for photoelectrochemical water splitting†

Thom R. Harris-Lee, [ab] Enrico Della Gaspera, [c] Frank Marken, [a] Jie Zhang, [b] Cameron L. Bentley [b] and Andrew L. Johnson *[a]

Aerosol-assisted chemical vapour deposition (AACVD) has been used in conjunction with new and bespoke precursors for the fabrication of highly nanostructured, mixed anatase-rutile phase TiO_2. Precursor syntheses were carried out in two steps, reacting tetrakis(dimethylamino)titanium with a triethanolamine-based ligand complex, followed by reaction with the relevant dry solvent. Suitability for AACVD was assessed by thermogravimetric analysis, and the resulting TiO_2 films were characterised by SEM, EDX, Raman, and PXRD, which was used to find relative ratios of anatase and rutile phase in the mixed-system, and respective grain sizes. The resulting TiO_2 films show exceptional OH^- oxidation performance under simulated solar irradiation, yielding photocurrent densities of 1.06 mA cm^{-2} at 1.23 V *vs.* RHE, and a peak incident photon conversion efficiency of 95.6% at 380 nm incident light, indicating their promise for use in photoanodes for water splitting application.

Introduction

Photoelectrochemical (PEC) water splitting is a promising method for efficient green hydrogen production, with most research focused on the rate limiting oxygen evolution reaction (OER) at the photoanode.[1] One standout material for use in photoanodes is titanium dioxide (TiO_2), owing to its low cost, non-toxicity, high photostability, and high catalytic activity with proper band edge positioning, however it is limited by its large bandgap (3–3.2 eV) and rapid recombination rate.[2] It is therefore likely that TiO_2 will be a key component in any future commercial PEC device, however it will need to be used in conjunction with other semiconductor layers and/or metal hybrids to overcome its limitations.[3]

Crystalline TiO_2 can exist in two photochemically active phases, anatase and rutile, with bandgaps of 3.2 and 3.0 eV respectively. While rutile is the more thermodynamically favoured structure, and possesses the narrowest bandgap, anatase is considered the more photochemically active form.[4] In fact, the best performing un-doped TiO_2 photoanodes have been reported to consist of both anatase and rutile phases, combining the best attributes of each material (increased photon absorption by virtue of the narrower rutile bandgap and an enhanced photochemical activity from anatase phase material). These features are further enhanced with the formation of a type II heterojunction, greatly improving charge separation, and reducing recombination.[5]

Aerosol-assisted chemical vapour deposition (AACVD) is a scalable and commonly used method for the fabrication of thin films for a diverse array of inorganic materials. In AACVD-based processes, chemical precursors need not be volatile, but merely soluble in any solvent from which the aerosol can be generated. As the requirement of volatility and thermal stability of precursors become less stringent, it is possible to produce high-quality CVD products at a lower cost. Compared to the conventional CVD method, AACVD presents some key advantages: (a) wider choice of precursors, (b) simplification of the delivery process with higher deposition rates, (c) flexible deposition parameters, (d) simplified production of multicomponent thin films with precise stoichiometric control. As such, AACVD lends itself to the use of chemically and thermally robust precursors which may be key to creating a commercially competitive device.[6]

Herein, three new TiO_2 precursors (Fig. 1a) have been designed and synthesised for use in AACVD, focusing on molecular structure that allows for (i) good solubility in 'inert'

[a] *Department of Chemistry, University of Bath, Claverton Down, Bath, BA2 7AY, UK. E-mail: a.l.hohnson@bath.ac.uk*
[b] *School of Chemistry, Monash University, Clayton, Vic 3800, Australia*
[c] *School of Science, RMIT University, Melbourne, VIC, 3000, Australia*

† Electronic supplementary information (ESI) available: The experimental methods, detailed crystallographic discussion, TGA discussion, SEM, EDX, Raman, optical spectroscopy data, X-ray crystallography data, detailed grain size and phase ratio data, photoelectrochemical data. CCDC 2260244–2260247. For ESI and crystallographic data in CIF or other electronic format see DOI: https://doi.org/10.1039/d3ma00364g

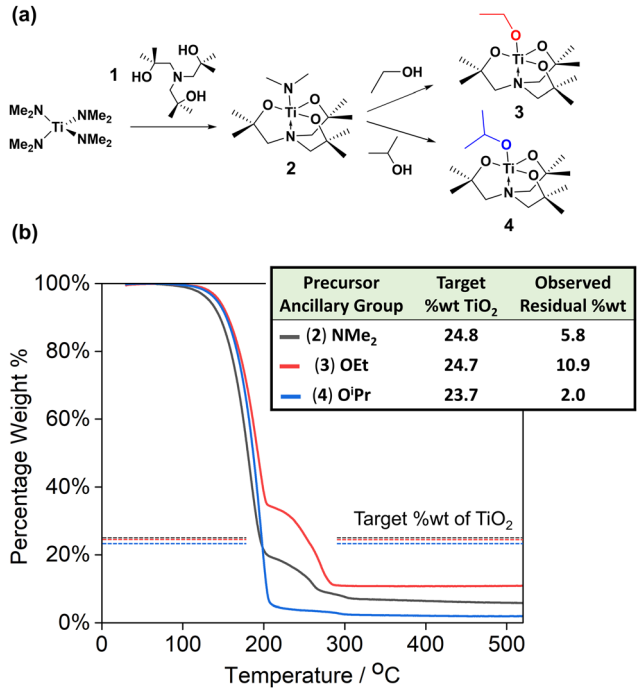

Fig. 1 (a) Reaction scheme for compounds **2**, **3**, **4**, (b) thermogravimetric analysis of compounds **2**, **3**, **4**, measured in an inert Ar glovebox atmosphere between 30 and 520 °C at a constant ramp rate of 5 °C min^{-1}, with target residual weight percentages marked using dotted lines, and compared to observed in the attached table.

solvents such as toluene, (ii) controllable and clean thermal decomposition pathways at practical temperatures, (iii) deposition of high surface area morphologies, (iv) adaptable ligand structures applicable to alternative metal centres to produce compatible metal oxide precursors. The molecular design also makes them more user-friendly and easier to handle than alternative purchasable TiO_2 precursors. Additionally, the resulting TiO_2 thin films are shown to contain mixed anatase-rutile phase, likely to be a significant influence towards the exceptional PEC performances measured for the TiO_2 films, and a rare property to obtain from a single-step deposition.

Results and discussions

The triethanolamine ligand (**1**), synthesised using a method adapted from Mun *et al.*,[1] and similar to work by Sharma *et al.*,[2] has been used to produce three different TiO_2 precursors by reaction of the pro-ligand **1** with $Ti(NMe_2)_4$ to yield the Ti(IV) amide complex **2** (Fig. 1a). Subsequent reaction of the mono-amide complex **2** with one molar equivalent of either anhydrous ethanol or anhydrous isopropanol resulted in the formation of the Ti(IV) alkoxide complexes **3** and **4** respectively. During the course of our investigations, the bridged-oxo complex, **5**, $[\{N(CH_2CMe_2)_3Ti\}_2(\mu\text{-}O)]$ was also isolated. Complexes **2–5** have been fully characterised by single crystal X-ray diffractometry and ^1H and $^{13}C\{^1H\}$ NMR spectroscopy (see ESI,† Sections S2 and S6).

Thermal characterisation of compounds **2**, **3**, and **4** was carried out using thermogravimetric analysis (TGA) (Fig. 1b). The onset decomposition temperatures (temperature after 1% mass loss) and end temperatures (after completion of a decomposition event) were recorded (Table S2, ESI†), as well as the TiO_2 target and experimental residual weight percentages (wt%). All three compounds showed lower residual wt% than expected for conversion to TiO_2, indicating a degree of volatility. However, it is interesting to note that the TGA plots of compounds **2** and **3** show secondary mass loss events starting at 210 and 227 °C respectively. This likely indicates both decomposition and volatilisation of the initial precursors are occurring simultaneously at temperatures below 210 (or 227) °C, while at higher temperatures only decomposition occurs. The final wt% of both **2** and **3** are above 0%, but significantly lower than the target residual mass corresponding to TiO_2, suggesting some by-product may be produced that has a vaporization (and decomposition) temperature greater than 520 °C. The final wt% for compound **4** (2.0%) is significantly lower than that expected for the formation of TiO_2 (23.7%), indicating a high degree of volatility. Based on TGA, all 3 compounds show suitability as AACVD precursors, however due to their increased air and moisture stability (Fig. S1, ESI†), complexes **3** and **4** were deemed to be the most promising precursors, and as such were used further in the AACVD of TiO_2 thin films.

For clarity of reading, thin films are denoted as TiO_2-X-Y, where X is the compound used as a precursor and Y is the deposition condition changed compared to the 'standard deposition procedure'; a deposition temperature of 450 °C, precursor concentration of 100 mM, and deposition time of 120 min. For example, a TiO_2 film deposited using **3** at 500 °C and otherwise standard conditions would be denoted as TiO_2-3-500 °C, while the film obtained using 'standard deposition procedure' is denoted TiO_2-3 (refer to Table S1, ESI† for the full sample list).

X-ray diffraction (XRD) patterns of TiO_2 thin films deposited using compounds **3** (Fig. 2a and Fig. S4a, b, ESI†) and **4** (Fig. 2b and Fig. S4c, d, ESI†) show a mixture of anatase and rutile phases, despite the single-step deposition process. This is promising for the application of these films in PEC devices as TiO_2 has been shown to have enhanced performance when both phases are present, as previously discussed. Anatase diffraction peaks are seen at approximately 2θ 25.3, 48.0, 55.1 and 62.8°, corresponding to (101), (200), (211) and (204) diffraction planes respectively, the (101) plane being the most intense, followed by (200). Rutile diffraction peaks are located at 2θ 27.4, 36.1, 54.3 and 69.0°, indexed to (110), (101), (211), (301) planes respectively, the (101) peak being the most intense, followed by (110).

Scanning electron microscopy (SEM) images (Fig. 2c and d and Fig. S2, ESI†) revealed all samples across both precursors had a similarly shaped nanostructure of tree-like rods extending perpendicular to the substrate surface. For compound **3**, there was no variation in rod size with precursor concentration; both TiO_2-3 and TiO_2-3-80 mM contained rods with 0.7–1.1 μm

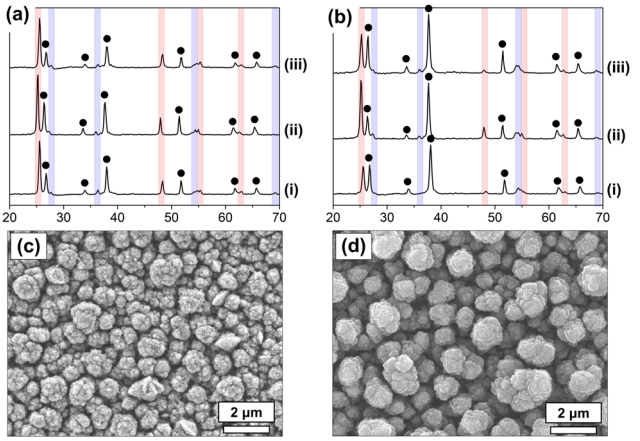

Fig. 2 (a) and (b) XRD patterns for TiO_2 films (a) (i) TiO_2-3-80 mM, (ii) TiO_2-3, (iii) TiO_2-3-120 mM, (b) (i) TiO_2-4-80 mM, (ii) TiO_2-4, (iii) TiO_2-4-120 mM. Peak locations corresponding to anatase and rutile phases are highlighted in red and blue respectively, and FTO is marked with a black dot. (c) and (d) Top-down electron micrographs of (c) TiO_2-3, (d) TiO_2-4.

diameter. Conversely, TiO_2-4 and TiO_2-4-80 mM consisted of rods with diameters of 1.0–1.3 μm and 0.5–0.9 μm respectively, evidencing the difference in deposition kinetics/pathway between the two precursors despite their similar molecular structures. All films were found to pass the 'Scotch tape test', and be strongly bound to the substrate, showing no obvious removal or damage.

Texture coefficients of the observed planes in the XRD spectra for both anatase and rutile, Table 1, were found using the Harris method[3] and powder diffraction standards for anatase (ICDD-JCPDS 75-1537) and rutile (ICDD-JCPDS 75-1748). The (101) XRD peak intensities for anatase phase showed no significant orientation preference compared to standard powder TiO_2, as indicated by texture coefficients shown in Table 1. The XRD (101) integrated peak area was therefore used to calculate anatase/rutile phase ratios. Volume average mean grain sizes were calculated (Fig. 3) using the most intense anatase and rutile peaks, (101), according to the equations:

$$X_A = [1 + K(I_R/I_A)]^{-1}; X_R = [1 - X_A], \quad (1)$$

$$\tau = [\kappa\lambda/\beta\cos\theta] \quad (2)$$

where X_R and X_A are the fractions of rutile and anatase phases respectively, I_A and I_R are the integrated areas of the most intense diffraction peaks for each anatase and rutile respectively, K is an empirical constant of value 0.79 calculated *via* XRD analysis on powders of pure rutile and anatase TiO_2, τ is the grain size, κ is the Scherrer constant equal to 0.94, λ is the X-ray wavelength used, β is the full width at half maximum (FWHM) of the most intense diffraction peak, and θ is the Bragg angle of the same peak.[9]

Table 1 Texture coefficients for TiO_2-3-80 and TiO_2-4

Anatase	TC(101)	TC(200)	TC(211)	TC(204)
TiO_2-3-80	0.96	1.04	0.65	0.85
TiO_2-4	1.07	0.93	0.78	1.05
Rutile	TC(110)	TC(101)	TC(211)	TC(301)
TiO_2-3-80	0.41	1.29	1.00	1.42
TiO_2-4	0.62	0.74	1.43	1.21

Fig. 3a illustrates that increasing the deposition time using complex **3** results in a larger grain size, minorly increasing for both anatase and rutile crystallites from 60 to 90 minutes, followed by a significant increase from 90 to 120 minute deposition. Unexpectedly, an increased deposition temperature of 500 °C showed smaller grain sizes for both phases (Fig. 3b), and a greater anatase percentage presence despite its metastability, usually transforming to rutile at high temperatures.[10] Except for the anatase grain size using 100 mM precursor, **3** showed little variation in grain sizes or phase composition as a function of precursor concentration (Fig. 3c).

Compound **4** showed significantly increase anatase phase fraction and grain size with increased deposition time (Fig. 3d). The rutile grain size calculated after a 60-minute deposition has been omitted due to its anomalous value (79.91 nm).

Increasing the deposition temperature (Fig. 3e) resulted in little change to anatase phase percent, contrasting to the relationship seen for compound **3**, however the crystallite grain sizes for both rutile and anatase phases appear to increase at higher deposition temperatures, consistent with previous observations. As can be seen from Fig. 3f, changes in the precursor concentration have little effect on phase composition of the resulting thin films for 80 mM and 100 mM, however there is an ~5% increase in rutile percent with 120 mM precursor, interesting as the respective grain sizes remain similar for all, except for the 100 mM rutile grain size. This is unlike the anatase phase, which does not show a similar change in composition.

As previously discussed, anatase-rutile mixed phase TiO_2 is consistently reported to improve PEC performance, however the optimum ratio can vary greatly between systems. UV/Vis spectroscopy was used to determine band gaps for TiO_2-3-80 and TiO_2-4 by Tauc analysis (Fig. S6, ESI†), resulting in a band gap of ~3.08 eV, close to both anatase (~3.2 eV) and rutile (~3.0 eV),[4] and consistent with both phases being present in the films. Given how close anatase and rutile band gaps are to one another, it is not expected to see two distinct transitions here. PEC analysis on all TiO_2 films developed here was therefore required to determine the optimum AACVD deposition conditions, how grain size and phase fractions impact performance, and compare the precursors in application (Fig. S7 and S8, ESI†).

TiO_2-3 showed higher photocurrent density compared to TiO_2-3-500 °C, while TiO_2-3-400 °C resulted in no visible deposition. It should be noted that these temperatures are not the exact temperature of the substrate due to the cooling effect of the argon and aerosol flow, however it was not possible to monitor the extent of this on the hot-wall AACVD setup.

Photocurrent densities of samples using **3** suggest less TiO_2 deposition gives enhanced performance, evidenced by TiO_2-3-80 mM and TiO_2-3-60 min (Fig. 4a and Fig. S7b, ESI†), the lowest precursor concentration and deposition time

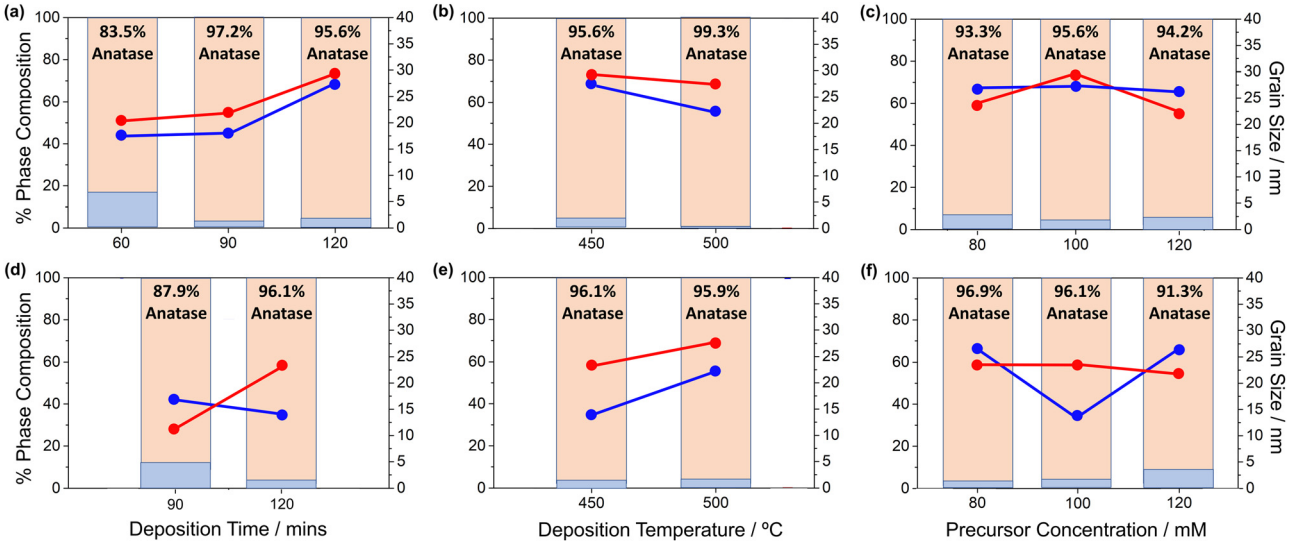

Fig. 3 Percentage compositions (bars, left axis) and crystallite grain sizes (lines, right axis) of anatase (red) and rutile (blue) in TiO_2 films deposited using (a)–(c) compound **3**, (d)–(f) compound **4**, as a function of (a) and (d) deposition time, (b) and (e) deposition temperature, (c) and (f) precursor concentration. Numerical anatase percent composition is shown in boxes.

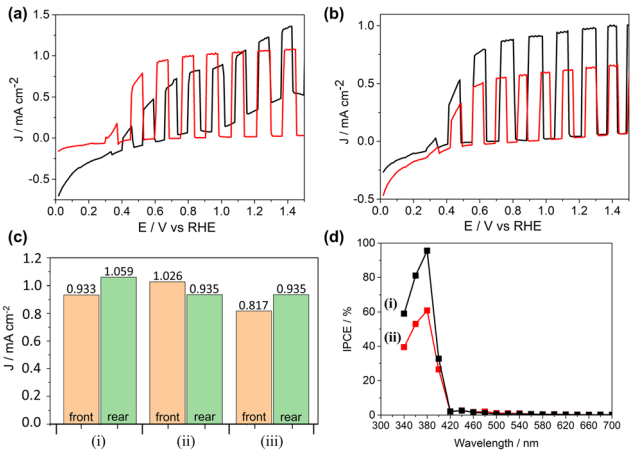

Fig. 4 (a) and (b) Linear sweep voltammograms of (a) black = TiO_2-3, red = TiO_2-3-80 mM, (b) black = TiO_2-4, red = TiO_2-4-80 mM, under 1 sun chopped AM 1.5 rear illumination; (c) Photocurrent densities at 1.23 V_{RHE} for the highest performing TiO_2 thin films: (i) TiO_2-3-80 mM, (ii) TiO_2-3-60 min, (iii) TiO_2-4; (d) incident photon-electron conversion efficiencies measured at 1.23 V *vs.* RHE for (i) TiO_2-3-80 mM, (ii) TiO_2-4. All measurements performed in 1 M KOH (pH 13.7) with a 15 mV s^{-1} scan rate.

respectively, displaying the greatest photocurrent densities of all those tested. Interestingly, for both these films, the front and rear side illuminated values are similar, suggesting that there are no limitations due to bulk charge transport within the TiO_2 material. Conversely, the photocurrent density of TiO_2-3 has a greater rear-side illumination performance than front-side (0.822 and 0.672 mA cm^{-2} respectively) indicating that electron mobility is limiting the photocurrents in the thicker films only. An area of ongoing work with these electrodes is in cation doping to improve bulk charge transport, enhancing the performance of thicker films to equal or surpass the best performing thinner ones here. Films deposited using compound 3 show clear correlation between increasing photocurrent density and increasing fraction of rutile phase for both precursor concentration ($j_{80\ mM} > j_{120\ mM} > j_{100\ mM}$; 6.7, 5.8, 4.4% rutile respectively) and deposition time ($j_{60\ min} > j_{120\ min} > j_{90\ min}$; 16.5, 4.4, 2.8% respectively).

All films deposited using compound **4** had a greater rear-side performance than front, indicating poor bulk charge transport properties. Similarly thin films deposited using **3** at 450 °C were shown to have an improved performance compared to those deposited and 500 °C particularly with respect to rear illumination, however, deposition times of 120 min were superior to those deposited over 90 and 60 min respectively, which showed no visible evidence of deposition.

The differences in deposition between **3** and **4** is highlighted by opposing optimal precursor concentrations, 80 mM showing the best performance for **3**, but 100 mM best for **4**. The anatase/rutile percentage compositions are similar for both precursors at 100 mM, however the anatase/rutile grain sizes for TiO_2-3 are significantly larger than TiO_2-4 (29.25/27.44 nm and 23.32/13.69 nm respectively). Additionally, TiO_2-4, the highest performing film for **4**, possessed both a smaller rutile grain size relative to all other films, but also a large difference between anatase and rutile sizes. This matches previous literature which has reported the benefits of small rutile grain sizes in mixed systems, forming more intimate contact with anatase grains, allowing for more rapid electron injection across the interface, enhancing charge separation, and reducing recombination.[5]

Linking photocurrent density to anatase/rutile phase composition of the best performing samples (Fig. 4c), TiO_2-3-80 mM and TiO_2-3-60 min surprisingly had significantly different rutile percentages, 6.7 and 16.5% respectively, while TiO_2-4 contained an even lower rutile fraction of 3.9%. Despite its notable impact, it is impossible to predict the phase ratios that will

Table 2 Comparing the PEC water splitting performance of TiO_2 thin films described here to the highest performing examples reported previously, as well as samples developed specifically using AACVD technique. Abbreviations: A = anatase, R = rutile, H = hydrogen

Synthetic route	TiO_2 phase	J^a/mA cm^{-2}	IPCE^b	$V_{on}{}^c/V_{RHE}$	Additional notes	Ref.
AACVD	93.3% A, 6.7% R	1.06	70% 95.6% (380 nm peak)	0.20	New precursor	Here
Anodization	100% R	H anneal: 2.50	98%	0.10	H annealed	8
		Air anneal: 0.60	2%	0.15		
Nanowire dropcast	80% A, 20% R	2.60	90%	n/a	H annealed	9
PP-MOCVD	91% A, 9% R	1.20	85%	0.1		7
Hydrothermal	A/R layered	1.10	57%	0.0	R rods with A branches	10
Anodization	100% A	1.59	n/a	0.25		11
Hydrothermal	100% R	H anneal: 1.25	22.5%	0.10	H annealed	12
		Air anneal: 0.65	10%			
AACVD	100% A	0.20	n/a	n/a		13
AACVD	100% A	0.67	100%	0.05	New precursor	4

^{a} Photocurrent density measured at 0 V *vs.* RHE under 1 sun (100 mW cm^{-2}, AM 1.5G) solar simulation. ^{b} IPCE measured at 350 nm incident photons, unless stated otherwise. ^{c} Photocurrent onset potential, measured *versus* RHE.

result from an untested deposition of these precursors, nor what the optimum ratio will be for a given precursor.

The onset potential (V_{on}) for TiO_2-3-80 mM was 0.05 V more positive than that for TiO_2-4, indicating that the charge transport within the sample deposited using precursor 3 had worse charge separation properties, despite its greater photocurrent at 1.23 V_{RHE}.

Incident photon-electron conversion efficiency (IPCE) measurements were carried out to further investigate photoelectronic properties of the films (Fig. 4d). The highest performing samples from **3** and **4**, TiO_2-3-80 mM and TiO_2-4, were measured, with IPCE values peaking at 380 nm (95.6% and 60.9% respectively) in both cases, followed by a rapid drop to negligible values at, and beyond, 420 nm. While the trend matches what is expected for the relatively wide band gap of TiO_2, peak conversion efficiencies are significantly higher than the 350 nm peak commonly seen. Reports of TiO_2 with similarly high efficiencies have often been further modified post-deposition, either by hydrogen or vacuum annealing,[5,6] or by formation of a second TiO_2 phase in a separate deposition process to obtain mixed anatase-rutile composition.[7]

Chronoamperometry over a 3 hour period has been used to determine photoanode stability. The absence of significant performance decrease over this period, as shown in Fig. S9 (ESI†), indicated no discernible change in the sample that would photocurrent drop-off. We therefore conclude that photocurrent densities are a direct consequence of OER from oxidation of OH^- species, rather than any potential self-oxidation of the photoanode (*e.g.* Ti(III) to Ti(IV) species).

A summary of the highest performing TiO_2 thin films for PEC application from literature have been outlined in Table 1, alongside the highest performing sample reported here (TiO_2-3-80 mM). Uniquely for TiO_2 films, the IPCE value for both TiO_2-3-80 mM and TiO_2-4 peaked at 380 nm, compared to the usual 350 nm peak reported.

The highest performing samples that have been reported previously use TiO_2 films that have been annealed in a reducing hydrogen environment. The next best samples commonly consist of mixed anatase-rutile phase TiO_2, combining the best properties from each material (smaller rutile bandgap, higher anatase activity), and forming intrinsic heterojunctions to improve charge separation. For further context, while Degussa P25 TiO_2 nanoparticles are commercially used in photocatalysis, we are unable to provide a direct comparison with these commercial materials as j and V_{on} metrics for these materials are not readily available.

All samples reported in this article were annealed in air at a relatively low temperature of 550 °C, therefore despite the hydrogen-annealed samples in Table 2 showing higher photocurrent densities, the films outlined here far outperformed those same samples when air annealed instead. The effect of H-annealing, as well as previously studied vacuum annealing,[6,14] will be investigated as part of ongoing work on these films, and other metal oxide films developed in a similar manner.

It is interesting that the rutile phase ratio for TiO_2-3-80 mM (6.7% rutile) was very similar to that reported by Krumdiek *et al.*,[7] another mixed phase film deposited using a CVD technique. The ability to fabricate competitive films using CVD, particularly AACVD, is vital for scale-up and commercialisation of such devices due to the scalability, versatility, and cost-effectiveness of the technique, especially when deposited in a single deposition step as is achieved here.

Conclusions

In summary, high performance, highly nanostructured, mixed anatase-rutile phase TiO_2 films have been produced using new precursors tailor-made for AACVD application in a single-step deposition procedure, outlining the importance of molecular precursor design in the development of photoelectrochemical materials and devices. The differences in performance, phase composition, grain sizes, and photoelectrochemical properties between the films deposited using different precursors evidenced the significant impact of small structural differences in precursor molecular design. These precursors (**3** and **4**) both had the valuable property of depositing mixed phase anatase-rutile films in a single deposition step, enhancing both PEC performance, and scale-up and commercial viability. This is

important work in the development of a 'toolbox' of bespoke metal oxide precursors systematically designed for AACVD that can be used to produce high performance metal oxide films and are also cross-compatible for the fabrication of mixed-metal and doped photoelectrodes in single-step depositions.

Experimental

Full experimental details for the synthesis and characterisation of the pro-ligand, **1**, as well as the Ti(IV) complexes **2**, **3**, **4** and **5** are included in the electronic supplementary information associated with this manuscript. Characterisation data includes ^{1}H and ^{13}C NMR data for **1–5** and single-crystal X-ray data for complexes **2–5**. Experimental details relating to the single-crystal X-ray crystallographic studies for compounds **2–5** are summarised in the ESI.†

Experimental procedure and thermogravimetric data for the complexes **2–4** is included in the ESI.† The ESI† also includes a comprehensive table of deposition conditions and sample notation, along with experimental procedure and results for the thin film characterisation, including SEM, EDX spectroscopy, PXRD, Raman spectroscopy, optical spectroscopy, photoelectrochemical characterisation of the thin TiO_2 thin films (including photocurrent density data).

Author contributions

T. R. Harris-Lee and A. L. Johnson prepared the original draft; F. Marken, J. Zhang, C.L. Bentley and A. L. Johnson reviewed and edited the article; T. R. Harris-Lee carried out the precursor synthesis, deposition experiments and photoelectrochemical characterisation; A. L. Johnson collected and processed all single crystal X-ray data. E. Della Gaspera conducted UV-Vis measurements and determined the band gap values. All authors approved the final manuscript.

Conflicts of interest

There are no conflicts to declare.

Acknowledgements

This work has been supported by the Institute for Sustainability, University of Bath, and Monash University, both of which are thanked for the provision of a joint Bath-Monash Global PhD studentship to T. R. H-L. C. L. B. is the recipient of an Australian Research Council (ARC) Discovery Early Career Researcher Award (DECRA, project number DE200101076), funded by the Australian Government. The authors acknowledge the use of the instruments and scientific and technical assistance at the Monash Centre for Electron Microscopy, a Node of Microscopy Australia. The authors gratefully acknowledge the Material and Chemical Characterisation Facility (MC^2) at the University of Bath, **https://doi.org/10.15125/mx6j-3r54**, for technical support and assistance in this work.

Notes and references

1 S. Deok Mun, J. Lee, S. H. Kim, Y. Hong, Y. Ho Ko, Y. K. Shin, J. H. Lim, C. S. Hong, Y. Do and Y. Kim, *J. Organomet. Chem.*, 2007, **692**, 3519–3525.
2 P. Sharma, S. K. Tripathi and P. Jaiswal, *IOP Conf. Ser.: Mater. Sci. Eng.*, 2021, **1136**, 012054.
3 G. B. Harris, *Philos. Mag. A J. Theor. Exp. Appl. Phys.*, 1951, **43**, 113–123.
4 M. Regue, S. Sibby, I. Y. Ahmet, D. Friedrich, F. F. Abdi, A. L. Johnson and S. Eslava, *J. Mater. Chem. A*, 2019, **7**, 19161–19172.
5 G. Wang, H. Wang, Y. Ling, Y. Tang, X. Yang, R. C. Fitzmorris, C. Wang, J. Z. Zhang and Y. Li, *Nano Lett.*, 2011, **11**, 3026–3033.
6 T. R. Harris-Lee, Y. Zhang, C. R. Bowen, P. J. Fletcher, Y. Zhao, Z. Guo, J. W. F. Innocent, S. A. L. Johnson and F. Marken, *Electrocatalysis*, 2021, **12**, 65–77.
7 A. J. Gardecka, C. Bishop, D. Lee, S. Corby, I. P. Parkin, A. Kafizas and S. Krumdieck, *Appl. Catal., B*, 2018, **224**, 904–911.
8 G. Wang, H. Wang, Y. Ling, Y. Tang, X. Yang, R. C. Fitzmorris, C. Wang, J. Z. Zhang and Y. Li, *Nano Lett.*, 2011, **11**, 3026–3033.
9 M. Liu, N. De Leon Snapp and H. Park, *Chem. Sci.*, 2011, **2**, 80–87.
10 J. Liu, X. Yu, Q. Liu, R. Liu, X. Shang, S. Zhang, W. Li, W. Zheng, G. Zhang, H. Cao and Z. Gu, *Appl. Catal., B*, 2014, **158–159**, 296–300.
11 Z. Zhang and P. Wang, *Energy Environ. Sci.*, 2012, **5**, 6506–6512.
12 J. Park, S. Lee, T. H. Lee, C. Kim, S. E. Jun, J. H. Baek, J. Y. Kim, M. G. Lee, S. H. Ahn and H. W. Jang, *Nano Convergence*, 2022, **9**, 1–14.
13 A. A. Tahir, T. A. N. Peiris and K. G. U. Wijayantha, *Chem. Vap. Deposition*, 2012, **18**, 107–111.
14 T. R. Harris-Lee, S. A. L. Johnson, L. Wang, P. J. Fletcher, J. Zhang, C. Bentley, C. R. Bowen and F. Marken, *New J. Chem.*, 2022, **46**, 8385–8392.